Effect of Glycans and the Glycophosphatidylinositol Anchor on Strain Dependent Conformations of Scrapie Prion Protein: Improved Purifications and Infrared Spectra

ARTICLE *in* BIOCHEMISTRY · MAY 2011

Impact Factor: 3.02 · DOI: 10.1021/bi2003907 · Source: PubMed

8 AUTHORS, INCLUDING:

Gerald S Baron
U.S. Department of Health and Human Services
41 PUBLICATIONS **2,389** CITATIONS
SEE PROFILE

Andrew G Hughson
National Institutes of Health
20 PUBLICATIONS **1,201** CITATIONS
SEE PROFILE

Published in final edited form as:
Biochemistry. 2011 May 31; 50(21): 4479–4490. doi:10.1021/bi2003907.

Effect of Glycans and GPI Anchor on Strain Dependent Conformations of Scrapie Prion Protein: Improved Purifications and IR Spectra†

Gerald S. Baron[*,‡], **Andrew G. Hughson**[‡], **Gregory J. Raymond**[‡], **Danielle K. Offerdahl**[‡], **Kelly A. Barton**[‡], **Lynne D. Raymond**[‡], **David W. Dorward**[§], and **Byron Caughey**[‡]

[‡]Laboratory of Persistent Viral Diseases, Rocky Mountain Laboratories, National Institute of Allergy and Infectious Diseases, National Institutes of Health, Hamilton, MT 59840

[§]Microscopy Unit, Research Technology Branch, Rocky Mountain Laboratories, National Institute of Allergy and Infectious Diseases, National Institutes of Health, Hamilton, MT 59840

Abstract

Mammalian prion diseases involve conversion of normal prion protein, PrP^{C}, to a pathological aggregated state (PrP^{res}). The 3D structure of PrP^{res} is not known but infrared (IR) spectroscopy has indicated high, strain-dependent beta sheet content. PrP^{res} molecules usually contain a glycophosphatidylinositol (GPI) anchor and large Asn-linked glycans, which can also vary with strain. Using IR spectroscopy, we tested the conformational effects of these post-translational modifications by comparing wild type PrP^{res} with GPI- and glycan-deficient PrP^{res} produced in GPI-anchorless PrP transgenic mice. These analyses required the development of substantially improved purification protocols. Spectra of both types of PrP^{res} revealed conformational differences between the 22L, ME7 and Chandler (RML) murine scrapie strains, most notably in bands attributed to beta sheets. These PrP^{res} spectra were also distinct from those of the hamster 263K scrapie strain. Spectra of wild type and anchorless 22L PrP^{res} were nearly indistinguishable. With ME7 PrP^{res}, modest differences between the wild type and anchorless spectra were detected, notably a ~2-cm^{-1} shift in an apparent beta sheet band. Collectively, the data provide evidence that the glycans and anchor do not grossly affect the strain-specific secondary structures of PrP^{res}, at least relative to the differences observed between strains, but can subtly affect turns and certain beta sheet components. Recently reported H/D exchange analyses of anchorless PrP^{res} preparations strongly suggested the presence of strain-dependent, solvent-inaccessible beta core structures throughout most of the C-terminal half of PrP^{res} molecules, with no remaining alpha helix. Our present IR data provide evidence that similar core structures also comprise wild type PrP^{res}.

The structure of the infectious, pathological form of prion protein (PrP^{res} or PrP^{Sc})[1] has been an enduring mystery for decades. During the course of transmissible spongiform encephalopathies (TSEs) or mammalian prion diseases, PrP^{res} is formed from the host's normal prion protein, PrP^{sen} or PrP^{C}, in a process that involves oligomerization and massive conformational change. PrP^{C} is largely alpha helical and disordered (1-3), while PrP^{res} is an ill-defined, often fibrillar multimer that is rich in beta sheet (1;4-6). Whereas the three-

†This research was funded by the Intramural Research Program of the National Institute of Allergy and Infectious Diseases, National Institutes of Health.

*To whom correspondence should be addressed. Phone: (406)-363-9485. Fax: (406)-363-9286. gbaron@niaid.nih.gov .

SUPPORTING INFORMATION AVAILABLE Supporting Figures 1 and 2 as mentioned in the text. This material is available free of charge via the Internet at http://pubs.acs.org.

dimensional structures of different PrP^C molecules have been determined by solution NMR (7) and X-ray crystallography (8), detailed structural analyses of PrP^{res} have been confounded by its insoluble multimeric properties. Rough secondary structure compositions of PrP^{res} have been estimated by infrared (IR) (1;4;5;9) and circular dichroism spectroscopic studies (6). IR (9-11) and a variety of biochemical measurements (12-20) have also indicated the existence of prion strain-dependent conformations of PrP^{res}. Electron crystallography on two-dimensional arrays present in certain PrP^{Sc} preparations has given additional low-resolution maps of an apparent nonfibrillar PrP^{res} ultrastructure (21;22). The strain-dependent dimensions of fibrillar PrP^{res} ultrastructures have been determined by electron microscopy and atomic force microscopy (23).

During biosynthesis, PrP^C is usually modified by the addition of up to two structurally diverse Asn-linked glycans (24;25) and a glycophosphatidylinositol (GPI) anchor (26). These post-translational modifications are often retained upon conversion of PrP^C to PrP^{res}. One of the well-documented strain-dependent variables in PrP^{res} structures is the relative proportion of singly glycosylated, doubly glycosylated, and unglycosylated molecules (i.e., glycoforms) in PrP^{res} aggregates from a given source (12;13;17;18;27). Moreover, studies with transgenic mice or cells expressing PrP^C mutants lacking one or both of the Asn-linked glycosylation sites have shown striking strain-dependent effects on prion disease susceptibility and pathogenesis (28-30). Such observations suggest that glycans might modulate PrP^{res} conformations, or that PrP^{res} conformers might vary in their propensities, or abilities, to incorporate differentially glycosylated PrP^C molecules. There is evidence of the latter possibility from studies of PrP^{res} formation in vitro (27;31) and in scrapie-infected cells (32). On the other hand, another report has suggested that glycosylation may not be necessary for strain-specific differences in PrP^{res} conformation, based on the location of proteinase K digestion sites (33). In any case, no higher resolution structural comparisons have been made to directly investigate the impact of glycosylation on PrP^{res} conformation for a given strain.

Removing the GPI anchor of PrP can also have dramatic effects on prion disease pathogenesis. Transgenic mice expressing PrP^C that lacks the C-terminal GPI anchor signal peptide (anchorless PrP^C) can be infected intracerebrally with prions, but the resulting disease (called fatal transmissible amyloid encephalopathy) is more like a cerebral amyloid angiopathy than a typical TSE disease (34;35). Interestingly, the absence of GPI-anchored PrP^C in these mice also nearly eliminates prion neuroinvasion and neural spread from more peripheral sites of inoculation (36). Anchorless PrP^C that is expressed in transgenic mice and in cell cultures is deficient in Asn-linked glycans (34;37). The reason for this is unclear, but presumably reflects an important role for membrane anchoring for proper glycosylation during biosynthesis (38). Consequently, when infected with mouse scrapie prions, these

[1]Abbreviations:

CBS	citrate-buffered saline
DRM	detergent-resistant membrane
GPI	glycophosphatidylinositol
PK	proteinase K
PrP^C	normal cellular prion protein
PrP^{res}	protease-resistant, disease-associated isoform of prion protein
rPrP	recombinant prion protein
TSE	transmissible spongiform encephalopathy

transgenic mice produce PrP^{res} that is both lacking the GPI anchor and severely underglycosylated.

The recent availability of anchorless, as well as wild type, PrP^{res} now permits analyses of the influence of glycans and GPI anchors on PrP^{res} structures. Because IR spectroscopy is capable of discerning prion strain-dependent variations in PrP^{res} secondary structures (9-11;39), it is probably the best available method for detecting conformational effects of these post-translational modifications on PrP^{res} strains. The amide I region (~1600-1700 cm^{-1}) of protein IR spectra reflects vibrational absorbances by the amide linkages that comprise the polypeptide backbone. The frequencies of these absorbances are modulated by transition dipole couplings and by hydrogen bonds between backbone amide protons and carbonyl oxygens of different amino acid residues, which, in turn, are determined primarily by various secondary structures. One practical obstacle to comparisons of anchorless and wild type PrP^{res} by IR has been difficulties in obtaining wild type murine scrapie PrP^{res} preparations of sufficient purity. In the present study we describe new improved purification protocols for different strains of anchorless and wild type PrP^{res} and their conformational comparisons by IR spectroscopy.

EXPERIMENTAL PROCEDURES

Purification of detergent-resistant membrane (DRM) PrP^{res}

The term detergent-resistant membrane (DRM) PrP^{res} refers to the use of brain DRMs as a starting subcellular fraction from which the PrP^{res} is subsequently purified. Wild type PrP^{res} was purified from Syrian Golden hamsters infected with the 263K scrapie strain or mice infected with the 22L or ME7 scrapie strains. Brains were dissected from animals exhibiting clinical scrapie signs, rinsed in PBS, blotted on filter paper to remove excess blood, snap frozen in liquid nitrogen, and stored at −80°C until needed. To isolate DRM PrP^{res}, brains were first thawed and rinsed in cold CBS (20 mM citrate/137 mM NaCl, pH 6.0). A 10% brain homogenate was then prepared from ~2 g of tissue by Dounce homogenization in CBS. In certain preparations the homogenate was centrifuged at 1000 *g* for 5 min at 4°C to remove large insoluble material. The supernatant was then subjected to Brij-96 (Fluka) extraction as described below. This optional centrifugation step had no noticeable effect on the purity of the final product nor on the IR spectra of DRM PrP^{res} (data not shown) but could reduce the yield of DRM PrP^{res} depending on the strain. The reduced yield was due to unexpected localization of the majority of the PrP^{res} to the 1000 *g* pellet fraction for certain strains such as 22L (data not shown). Therefore, we recommend either omitting this centrifugation step or analyzing the partitioning of PrP^{res} and optimizing Brij-96 extraction conditions for strains not described here. The homogenate was rapidly and thoroughly mixed on ice with one volume of ice-cold 1% Brij-96 (in CBS) and incubated on a rotisserie at 4°C for 30 min. After Brij-96 extraction, the sample was adjusted to 26% OptiPrep (in 10 mM citrate/137 mM NaCl, pH 6.0) and split equally across 6 pre-chilled centrifuge tubes. This fraction was overlaid with layers of 23% (12 ml) and 8% (8 ml) OptiPrep (in 10 mM citrate/137 mM NaCl, pH 6.0) followed by 1 ml of 10 mM citrate/137 mM NaCl (pH 6.0). The gradients were centrifuged in a pre-chilled Beckman SW32 rotor at 18500 rpm for 2 hr at 4°C. Prominent lipid bands were visible at the CBS/8% OptiPrep and 8%/23% OptiPrep interfaces, the latter representing the PrP^{res}-enriched fraction. The layers above the 8%/23% lipid band were carefully aspirated and discarded prior to careful collection of the lipid band at the 8/23% interface, which we refer to as the DRM fraction.

The second portion of the procedure involved extraction and purification of PrP^{res} from the DRM fraction. After equilibrating the sample to room temperature (RT), a high salt extraction was performed on the DRM fraction by adding ½ volume of 5 M NaCl (in 0.15 M Tris, pH 8.0), mixing thoroughly, and incubating for 15 min at RT. The high salt-washed

DRMs were split to 4 tubes and fractionated on a second floatation gradient consisting of a bottom fraction of salt-extracted DRMs adjusted to 26% OptiPrep (from a 60% stock) and overlaid with ~1/4 volume (~7 ml) of 23% OptiPrep in TBS (10 mM Tris/137 mM NaCl, pH 8.0) and 1 ml of TBS. The gradients were centrifuged in an SW32 rotor at 18500 rpm for 2 hr at 20°C. This high salt extraction was intended to disrupt electrostatic interactions between PrP^{res} and high molecular weight molecules such as glycosaminoglycans and ferritin (40) and remove some of these contaminants from the DRMs. The lipid band at the TBS/23% OptiPrep interface was carefully collected and adjusted to a final volume of 27 ml with TBS. To solubilize the membranes and digest nucleic acids, 3 ml of 20% sarkosyl/0.5 M Tris (pH 7.5) was added followed by Benzonase to a final concentration of 25 U/ml and incubation at 37°C for 30 min. The sample was then digested with 10 μg/ml PK for 1 hr at 37°C. PK digestion was terminated by addition of Pefabloc SC (2 mM final concentration) and incubation on ice for 15 min. To remove PK, the sample was first adjusted to 30 mM EDTA and incubated for 5 min at RT. Next, the sample was centrifuged at 1000 *g* for 5 min at RT to remove large insoluble material. The supernatant was adjusted to contain a final concentration of 1.8 M NaCl and the entire mixture was gently overlaid onto ½ volume of a sucrose pad solution (1 M sucrose/0.1 M NaCl/0.5% sulfobetaine 3-14/10 mM Tris, pH 7.5). After centrifugation in a Beckman Type 50.2 Ti rotor at 45000 rpm for 2 hr at 20°C, the supernatant was carefully removed without disturbing the pellet. The pellet was washed by resuspension in 3 ml of 0.5% sulfobetaine (in PBS) followed by centrifugation in a TLA100.3 rotor at 70000 rpm for 30 min at 4°C. The supernatant was thoroughly removed and the final DRM PrP^{res} pellet was resuspended in 0.5% sulfobetaine (in PBS) by pipetting and brief cuphorn sonication as needed. Yields of DRM PrP^{res} ranged from ~2.5-12.5 μg/g of brain for 22L and ME7 strains and ~25-50 μg/g of brain for 263K with the lower yields corresponding to preparations with homogenates subjected to the optional 1000 *g* clearing step above.

Purification of anchorless PrP^{res}

Brain homogenates from scrapie-infected $tg44^{+/+}$ transgenic mice (35) expressing GPI anchorless PrP^{C} were adjusted to contain 50 mM Tris/137 mM NaCl/2% sarkosyl (pH 8.0) (TBSS) and incubated for 20 min at room temperature (RT). After Benzonase treatment (25 U/ml, 30 min) to digest nucleic acids, the samples were centrifuged (Beckman Type 50.2 Ti rotor, 24 min, ~40500 g_{max}) to pellet the PrP^{res} and other detergent-insoluble material. These centrifugation conditions provided a k factor comparable to centrifugation at top speed in a Beckman microcentrifuge. The pellet was resuspended in TBSS carefully avoiding the brown portion of the pellet. The sample was then digested with proteinase K (PK) at 10 μg/ml for 1 hr. After termination of the PK digest, a PK-stripping procedure similar to that described previously (41) was performed by addition of EDTA (30 mM final concentration) and NaCl (1.7 M final concentration), layering onto a sucrose cushion (1 M sucrose, 100 mM NaCl/0.5% sulfobetaine 3-14/10 mM Tris, pH 7.4), and recovery of the PrP^{res} by centrifugation as above through the sucrose cushion. The pellet was then resuspended in 0.5% sulfobetaine 3-14 (in PBS) and centrifuged again in order to wash the pellet. The final PrP^{res} pellet was resuspended in a small volume of 0.5% sulfobetaine 3-14 (in PBS) with brief cuphorn sonication. The yields of anchorless PrP^{res} were ~168 μg/g of brain for 22L, ~123 μg/g of brain for Chandler (RML), and ~75 μg/g of brain for ME7. Control “mock” preparations from age-matched uninfected mice contained a small pellet of translucent material that was resuspended as described for the anchorless PrP^{res} pellets. A more detailed description of the purification procedure for anchorless PrP^{res} can be found elsewhere (42).

SDS-PAGE and immunoblotting

Samples were denatured by boiling 8-10 min in sample buffer (4 M urea/5% SDS/5% glycerol/3 mM EDTA/0.02% bromophenol blue/62.5 mM Tris, pH 6.8) with either DTT (50

mM) or β-mercaptoethanol (4%) as a reducing agent. As needed, samples were cuphorn sonicated in sample buffer to improve solubilization of highly stable protein aggregates. Proteins were separated on 10% Bis-Tris NuPAGE gels in MES running buffer. GelCode Blue staining was performed following the manufacturer's recommendations (Thermo Scientific). Silver staining was performed as described elsewhere (43). Purified mouse ferritin was purchased from Lee Biosolutions. The 90-231 fragment of hamster PrP (recPrP^{sen} 90-231) (predicted MW 16243 Da) was purified from *Escherichia coli* as described elsewhere (44) and used as a standard for quantitation of PK-treated anchorless PrP^{res}. For immunoblotting, proteins were transferred to PVDF membranes by a semi-dry method. For PrP immunoblots, prior to blocking the membranes were treated with either 0.2 M NaOH (30 min) or 3 M GdnSCN (10 min) followed by 4 rinses with TBS. Primary antibodies used for PrP detection included 6D11 (Covance Research Products) and R20 (rabbit polyclonal antiserum against PrP residues 218-232). Primary antibodies to detect ferritin included chicken anti-mouse ferritin (Immunology Consultants Laboratory) and rabbit anti-heavy chain human ferritin (Abcam #16875). Secondary antibodies were purchased from Jackson Immunoresearch (alkaline phosphatase conjugates) or Invitrogen (Alexa Fluor 488 conjugates). Alkaline phosphatase conjugates were detected using Attophos substrate (Promega). Alexa Fluor 488 conjugates were visualized by direct fluorescence. All blots were imaged on either a Storm or a Typhoon scanner (GE Healthcare).

Transmission electron microscopy

Samples were spotted onto Formvar and carbon-coated grids from Ted Pella (Redding, CA). For samples in Figure 1, grids were freshly glow-discharged. After allowing 30-60 min for adsorption, the grids were washed extensively with ultrapure water. The samples were then stained with either 1% methylamine tungstate (Nano-W from Nanoprobes, Yaphank, NY) or 1% ammonium molybdate where indicated. After drying, the samples were imaged at 80 kV on a Hitachi H7500 electron microscope equipped with an AMT XR-100 digital camera.

IR spectroscopy

IR spectra were obtained using a Perkin-Elmer Spectrum 100 instrument equipped with a diamond attenuated total reflectance sample unit and an MCT detector as described (42). Briefly, PrP^{res} aggregates in 0.5% sulfobetaine in PBS containing between 6-20 μg of protein were pelleted, washed with water, and resuspended as a 1-2 μl slurry. The slurry was applied to the diamond and dried to a film over a few minutes while following the disappearance of the broad liquid water band at ~1636 cm^{-1} and the appearance of the protein amide I and amide II bands. The spectra were background-subtracted and comprised of 64 accumulations (4 cm^{-1} resolution; 1 cm/sec OPD velocity; strong apodization) Those shown were collected as soon as successively collected spectra (each taking 80 sec) stabilized, indicating little further evaporation of liquid water. This approach was taken to essentially eliminate spectral contributions from free liquid water without desiccating the protein film any more than necessary. Second derivative spectra were calculated using the instrument software and 13 data points.

RESULTS

Purification of anchorless PrP^{res}

PrP^{res} accumulates in extraneural tissues in scrapie-infected tg44$^{+/+}$ transgenic mice expressing anchorless PrP (45). This provided several potential sources of tissue to use for the purification of anchorless PrP^{res}. To determine the optimal tissue for purification, we first used semi-quantitative immunoblotting to compare the levels of PrP^{res} in a selection of tissues reported to have the highest amounts of PrP^{res} (45). When samples were normalized

for total protein, brain and brown fat contained the highest reproducible levels of PrP^{res} (data not shown). Since there is more brain tissue available per animal than brown fat, brain contained the largest total amount of PrP^{res} and was therefore chosen as the starting material.

The purification procedure used for anchorless PrP^{res} preparations analyzed in the present study was based on methods previously described for purification of wild type (41) and anchorless (23) PrP^{res} with some important modifications as detailed under Experimental Procedures. Anchorless PrP^{res} was prepared from the brains of $tg44^{+/+}$ mice infected with the Chandler (RML), 22L, or ME7 strains of mouse scrapie. Analysis of the samples by transmission electron microscopy (TEM) showed that the PrP^{res} preparations were almost exclusively comprised of amyloid-like fibrils (Figure 1) as expected from previous studies (23;34), the exception being rare individual collagen fibers that were only detected with extensive searches of entire grids (data not shown). Collagen fibers were also present but infrequent in control "mock" PrP^{res} preparations from age-matched, uninfected $tg44^{+/+}$ mice (data not shown). Occasional clusters of electron dense particles were observed in mock and scrapie PrP^{res} preparations. Because these were also present in buffer control samples they were attributed to buffer components such as sulfobetaine (Figure 1, "Buffer control"). Extensive searches of anchorless and mock anchorless PrP^{res} samples failed to detect ferritin, a known contaminant of wild type PrP^{res} preparations (41;46) readily distinguished by its characteristic "fish-eye" appearance (Figure 1). Together, these observations established that the anchorless PrP^{res} preparations were highly enriched for amyloid-like fibrils.

Anchorless PrP^{res} preparations were further subjected to biochemical analyses to assess sample purity. Analysis by SDS-PAGE with silver staining showed that all anchorless scrapie PrP^{res} preparations were of high purity (Figure 2A, lanes 4-6). As previously reported (34), predominantly unglycosylated PrP was present accompanied by a lower level of monoglycosylated PrP (Figure 2A, lanes 4-6, bracket). Interestingly, anchorless ME7 PrP^{res} exhibited a higher apparent molecular mass compared to Chandler and 22L, suggesting anchorless ME7 PrP^{res} contains a larger PK-resistant core. This is consistent with data from mass spectrometric analysis (42). The bands present in anchorless PrP^{res} preparations were specific to scrapie-infected animals as shown by analysis of control mock preparations (Figure 2A, lanes 10-11). Ladders of higher molecular mass species observed by silver staining correlated with bands detected by immunoblotting with two different anti-PrP antibodies (Figure 2B, lanes 7-9 and 11-13), showing that the bands detected by silver staining primarily consist of SDS-resistant oligomers of anchorless PrP^{res}. In higher exposure images, low molecular mass bands were also visualized that were unique to each strain and antibody, thereby revealing further strain-specific differences between the various anchorless PrP^{res} aggregates (Figure 2B, brackets, lower panels). By comparison with $rPrP^{sen}$ 90-231 standards, we estimated the typical yields of anchorless PrP^{res} to be ~168 μg/g of brain for 22L, ~123 μg/g of brain for Chandler, and ~75 μg/g of brain for ME7.

Immunoblotting with an anti-heavy chain ferritin antibody was used to more sensitively assay for the presence of ferritin. Ferritin was readily detected in a standard wild type 22L PrP^{res} preparation (Figure 2C, lane 6). However, even when overloading the gel with ~4-7-fold more anchorless PrP^{res} (~1.2-2 μg) vs. wild type (300 ng), only a faint pair of bands were detected in two independent anchorless PrP^{res} preparations (Figure 2C). Similar results were obtained using a different anti-ferritin antibody, chicken anti-mouse ferritin (data not shown). Given the bands precisely co-migrate with anchorless PrP^{res} monomers and the signal is not competed in a control immunoblot using anti-ferritin antibody pre-adsorbed with purified ferritin (Figure 2C, compare lanes 4-5 with 10-11), these data show there is at most a negligible concentration of ferritin present in anchorless PrP^{res} preparations.

Altogether, these data establish the very high purity of the anchorless PrP^{res} preparations and allow their use in IR spectroscopy studies.

Purification of wild type PrP^{res} from detergent-resistant membranes

To develop an improved protocol for purification of wild type PrP^{res}, we investigated potential sources for molecules that are co-enriched with PrP^{res} in our standard preparation method (41) due to properties shared with PrP^{res} (i.e. detergent insolubility, protease-resistance, high density). Key insight was obtained from characterization of "mock" PrP^{res} preparations derived from uninfected, wild type animals analogous to the mock preparations from anchorless mice described above. First, ferritin-like particles were detected by electron microscopy (Supporting Figure S1A) independent of whether preparations were conducted with or without an optional PK treatment (41) during the preparation. Amorphous objects were also present but less frequent in PK-treated preparations (data not shown). Ferritin contamination was confirmed in mock, 22L, and 263K PrP^{res} preparations by immunoblotting with anti-ferritin antibody (Supporting Figure S1B). These data are consistent with independent studies (40;46). In addition to ferritin, other lower molecular mass proteins were detected in the standard mock PrP^{res} by GelCode Blue staining (Supporting Figure S1C) and silver staining (see below) with similar apparent molecular mass to proteins in scrapie PrP^{res} preparations that did not correspond to known PrP bands (see below). This indicated that several endogenous brain proteins can contribute to contamination of PrP^{res} preparations based on their inherent similarity to the biochemical and biophysical properties of PrP^{res}. This finding was supported by independent mass spectrometry studies (46).

This prompted us to identify biochemical features that might distinguish PrP^{res} from the mock PrP^{res} contaminants. We determined that the predominant mock PrP^{res} proteins lacked N-glycosylation and GPI anchors by digestions with PNGase F and phosphatidylinositol-specific phospholipase C (data not shown). Since PrP^{res} is GPI-anchored and associated with brain detergent-resistant membranes (DRMs) for multiple rodent scrapie strains (47-50) and (G. Baron, unpublished observations), this suggested that DRM fractionation could be used to separate PrP^{res} from many contaminants in PrP^{res} preparations and thus generate PrP^{res} preparations of higher purity.

Many factors such as type of detergent, detergent concentration, extraction temperature, and detergent:protein ratio can all influence the association of proteins with DRMs (51;52). Therefore, we tested two different detergents (Triton X-100 and Brij-96) and various extraction conditions and gradient profiles to optimize enrichment of PrP^{res} in DRMs. Although both detergents gave similar results, extraction with cold 0.5% Brij-96 produced slightly better results in small scale experiments (data not shown). As shown in Figure 3A, DRM fractionation of brains from 263K-affected hamsters and 22L-affected mice led to floatation of virtually all PrP^{res} in a lipid band of intermediate density consistent with DRMs (fractions 5-6). The distribution of total PrP in such gradients, as determined by immunoblotting samples without PK digestion, was identical to that of PrP^{res} (data not shown). A lower density lipid band corresponding to fractions 2-3 was also observed, but this did not contain detectable PrP^{res}. This membrane fraction may in part be derived from myelin membranes, which can exhibit some detergent-resistance (53). BCA protein assay of fractions from DRM floatation gradients showed that a substantial portion of the total protein was localized to the higher density bottom fractions with a much smaller amount corresponding to PrP^{res}-containing DRM fractions (Figure 3A, graph). These data established that DRM fractionation led to a significant enrichment of PrP^{res} over other brain proteins and biomolecules.

Because DRM fractionation alone would be insufficient to purify PrP^{res}, we designed a new purification procedure (described in Experimental Procedures) that incorporated DRM fractionation with elements of a standard PrP^{res} preparation method (41). For simplicity, we refer to preparations using this new method as DRM PrP^{res}. Silver stain SDS-PAGE analysis of DRM PrP^{res} preparations corresponding to the 263K, 22L, and ME7 scrapie strains showed dramatically reduced levels of the low molecular mass contaminants present in standard PrP^{res} preparations and standard mock PrP^{res} preparations (Figure 3B, brackets and arrows). Interestingly, a pellet of material is obtained in mock DRM PrP^{res} preparations. However, mock DRM PrP^{res} preparations essentially lacked any detectable proteins as compared with equal brain equivalents of standard mock PrP^{res} preparations (Figure 3B, compare lanes 3 vs. 4 and 7 vs. 8). Mock DRM PrP^{res} preparations are not devoid of protein as proteins can be detected in these preparations by loading much higher (~5-10-fold more) amounts, but the banding profile still differs from those in standard mock PrP^{res} preparations (data not shown). Although the molecular composition of the mock DRM PrP^{res} fraction remains to be determined, our data (here and see below) suggest it may contain lipids. Immunoblot analysis of DRM PrP^{res} preparations with an anti-PrP antibody showed a strong correspondence between immunoreactive bands and bands detected by silver staining, including those of both monomeric (arrows) and SDS-resistant oligomeric (brackets) PrP (Figure 3C). Ferritin contamination of DRM PrP^{res} preparations was also dramatically reduced compared to standard PrP^{res} preparations as shown in Figure 3D. Although ferritin was readily detectable by immunoblot analysis of standard 263K PrP^{res} (arrow), it was undetectable in a similar amount of 263K DRM PrP^{res}. Semi-quantitative analysis of ferritin content in 22L DRM PrP^{res} using two different anti-ferritin antibodies and ferritin standard curves estimated ferritin levels to be ~ 4.1 or 6.4 ng ferritin/150 ng PrP (lane 6 in Figure 3E and Supporting Figure S2). By contrast, a standard 22L PrP^{res} prep contained either 78 ng or 26 ng of ferritin/150 ng PrP depending upon the antibody used (lane 5 in Figure 3E and Supporting Figure S2). This corresponds to a 4.1 to 19-fold reduction in ferritin content. Since the DRM PrP^{res} preparations were PK-treated, we conducted control experiments to confirm that, as expected, pre-treating ferritin with PK digestion had a negligible effect on ferritin detection (lanes 1-4 vs. 7-10 in Figure 3E and Supporting Figure S2). TEM analysis of DRM PrP^{res} preparations showed they consisted of amyloid-like fibrils with rare collagen fibrils as seen with the anchorless PrP^{res} samples (Figure 4). The amyloid-like fibrils were absent from control mock DRM PrP^{res} preparations, which contained only rare collagen fibrils and vesicle-like structures and were detected only by loading 10 times the sample equivalents versus the 263K or 22L DRM PrP^{res} (Figure 4). Collectively, these observations provide strong evidence that the DRM PrP^{res} purification procedure was successful in generating sufficient yields of highly-purified PrP^{res} well-suited for IR spectroscopy and other applications.

IR spectra of anchorless PrP^{res}

IR spectra of multiple (at least two) independent 22L, ME7 and Chandler anchorless PrP^{res} preparations were compared to one another as well as to spectra of recombinant murine PrP^{sen} 90-231 and mock anchorless PrP^{res} preparations from uninfected $tg44^{+/+}$ mice. The upper half of Figure 5 shows the primary IR spectra and the bottom shows second derivative spectra calculated directly from the primary spectra. The second derivatives give negative peaks corresponding to maxima in the primary spectra and provide an unbiased enhancement of band resolution. Consistent with previously reported IR spectra of hamster (4;9-11) and murine PrP^{res} preparations (54), the most prominent absorptions were in a spectral region typically assigned to beta sheets, i.e. 1615-1636 cm^{-1}, indicating predominant beta sheet content. This high beta sheet absorbance was in striking contrast to the predominant absorbance maxima at ~1657 and 1650 cm^{-1} of the $rPrP^{sen}$ 90-231. The latter maxima were consistent with PrP^{sen}'s high alpha helical and disordered secondary

structures (2) and previously reported IR data (1;55). As has been reported for wild type PrP^{res} from hamsters (4;9-11) and mice (54), clear differences were observed between the different mouse strains of anchorless PrP^{res}, most notably in the beta sheet region of the second derivative spectra. These results provide direct evidence that strain-dependent differences in PrP^{res} secondary structure exist in the absence of GPI anchors and, for the most part, N-linked glycans.

Comparisons of anchorless and wild type PrP^{res}

To investigate whether glycans and anchors modify the secondary structures of PrP^{res}, we also collected IR spectra of fully glycosylated and GPI-anchored wild type DRM PrP^{res} of the 22L and ME7 strains prepared by the improved purification protocol described above. In addition, an analogous mock preparation from uninfected mouse brain tissue was also analyzed. As shown in Figure 6, the mock preparation gave a spectrum in the 1600-1700 cm^{-1} region that was considerably less intense than the corresponding PrP^{res} spectra. Moreover, the mock spectrum was broad and relatively featureless, and when subtracted from the PrP^{res} spectra (ME7-mock), had little impact on the features of their second derivative spectra. Another potential complication in comparing the IR spectra of the wildtype and anchorless PrP^{res} preparations is that N-acetyl glucosamine moieties in N-linked glycans and GPI anchors can also absorb near the beta sheet region (~1638 cm^{-1}) (4). However, their overall contributions to PrP^{res} spectra in this region should be minor (4). Indeed, the spectrum of the wild type 22L PrP^{res} was nearly indistinguishable from that of the anchorless 22L PrP^{res}, except for modestly enhanced absorbance centered at ~1670 cm^{-1}(Figure 7). The latter band is in the spectral region commonly ascribed to turn structures (39). In the case of ME7 PrP^{res}, differences between the wild type and anchorless structures were subtle, but more apparent than in the 22L PrP^{res} preparations. Most notable was a shift in the low-frequency beta sheet band from ~1620 cm^{-1} to ~1622 cm^{-1} with the post-translational modifications. Altogether the IR spectra of the anchorless and wild type PrP^{res} provide evidence that the N-linked glycans and GPI anchor do not grossly affect the strain-specific secondary structures of PrP^{res}, but may have subtle effects on turn (or perhaps loop structures) and, in the case of ME7, certain beta sheet components.

DISCUSSION

The present work provides the first direct evaluation of the effects of the GPI anchor and Asn-linked glycans on PrP^{res} conformation. Two recent developments have made these analyses possible: first, the recent availability of scrapie-infected transgenic mice expressing only anchorless PrP molecules which are also severely deficient in Asn-linked glycans (e.g. see predominance of lower, unglycosylated isoform in Figure 2A and 2B), and second, our new purification protocols for anchorless and wild type PrP^{res}. These protocols greatly reduce the presence of contaminants that, in hindsight, must have confounded previous IR analyses of wild type murine PrP^{res} (54) which, notably in the case of 22L PrP^{res}, gave spectra that are significantly different than those reported here. Contamination has been much less of a problem with certain hamster PrP^{res} preparations because of their much higher starting PrP^{res} content per mass of brain tissue. Nevertheless, improvements were observed when the DRM PrP^{res} method was applied to hamster 263K PrP^{res} as shown by the reduction in ferritin contamination (Figure 3B and 3D).

Our rationale for purifying wild type PrP^{res} starting with DRM membrane preparations rather than fully detergent-solubilized whole brain homogenates stemmed from the discovery that many contaminants present in preparations made using a standard method (41) seemed to correspond to endogenous brain proteins in mock PrP^{res} preparations with biochemical and biophysical properties similar to PrP^{res}. These properties included detergent-insolubility, protease-resistance, and high density. Working independently,

another group has identified some of the proteins present in both mock and wild type mouse PrP^{res} samples (46). We reasoned that some of these detergent-insoluble, high density contaminants might be separated from PrP^{res} by floatation of PrP^{res}-enriched DRMs on density gradients. To minimize co-enrichment for certain high molecular mass contaminants such as ferritin due to their direct association with PrP^{res} via electrostatic interactions (40), we performed a high salt treatment of the DRM fraction. This should disrupt these interactions and remove these contaminants by recovery of the salt-washed DRMs on a second floatation gradient. The high salt treatment is a component of a standard PrP^{res} purification procedure that is thought to remove some glycosaminoglycans (41). However, since this treatment is applied to a sarkosyl-extracted brain homogenate, high density molecules like ferritin that might become dissociated from PrP^{res} would still co-sediment with the PrP^{res} in the subsequent ultracentrifugation step. Because we have found that wild type PrP^{res} of many scrapie strains associates with the DRM fraction, including strains prone to generating large plaque-like PrP^{res} deposits (e.g. 87V, data not shown), it is likely our DRM PrP^{res} purification method is broadly applicable to purification of wild type GPI-anchored PrP^{res}.

Consistent with our rationale, at most very low levels of endogenous brain proteins were enriched in mock anchorless PrP^{res} preparations (Figure 2A). The accumulation of anchorless PrP^{res} in large amyloid deposits permitted the recovery of anchorless PrP^{res} at substantially lower centrifugation speeds than are used for wild type PrP^{res}. This could reduce the opportunity for co-purification of high molecular mass, dense, protease-resistant contaminants (e.g. ferritin). A further modification applied to both the new wild type and anchorless PrPres preparation procedures was the use of Benzonase to digest nucleic acids in place of sequential RNase A and DNase digestions. This avoided the use of RNase A which is partially resistant to PK digestion (56), forms aggregates under certain conditions (57;58), and thus could be a source of contamination.

Another group working in parallel has reported the use of DRM fractionation to enrich for PrP^{res} with the goal of generating antigen for immunizations to create anti-PrP antisera (50). Although these authors used DRM fractionation in the initial purification step, subsequent steps to further enrich for PrP^{res} were dramatically different from our method. Most importantly, the apparent purity of the PrP^{res} from this method was substantially lower than that shown in the present study as indicated by the presence of prominent silver-stained bands that were not reactive with anti-PrP antibodies (50). Moreover, only portions of the gels corresponding to a narrow apparent molecular mass range from ~20-50 kDa are shown (50). Hnasko et al. (2010) argue that the lack of induction of antibodies against other brain DRM proteins besides PrP provides evidence of the purity of their PrP^{res} preparations. However, this may simply represent murine immunological tolerance to these non-PrP rodent proteins just as they observed for PrP itself (i.e. no anti-hamster PrP antibodies were generated in immunizations of wild type mice). Although the PrP^{res} preparations of Hnasko et al. are useful for immunization experiments, they would not be of sufficient purity for IR analyses presented here.

Our study clearly reinforces previous reports of the ability of IR spectroscopy to detect differences in conformation between PrP^{C} and PrP^{res}, as well as between different PrP^{res} strains comprised of the same polypeptide precursor (9-11;39). Relative to those differences, the spectral effects of glycans and GPI anchors on PrP^{res} were modest (Figures 5-7). Clearly differences in beta sheet and apparent turn structures can be resolved between PrP^{res} strains of the same amino acid sequence, but there is always potential for spectral overlaps in IR amide I spectra of different polypeptide secondary structures. Thus, an inability to distinguish IR spectra does not guarantee the presence of identical secondary structures, and, subtle differences in secondary structures, i.e., involving only a few residues, might also be

difficult to detect. Nonetheless, the most straightforward interpretation of the present IR data is that glycans and anchors do not cause gross conformational changes that are commensurate with the differences between PrP^{res} strains, especially in the case of 22L PrP^{res}. A more noticeable effect of these post-translational modifications was seen with the ME7 strain, but much of the spectrum remained unchanged.

Given the apparently tight packing of PrP molecules in PrP^{res} fibrils, as evidenced by their resistance to proteinase K digestion and H/D exchange (42), one can imagine that the presence of bulky post-translational modifications might not only affect monomer conformations, but also constrain the options for packing PrP monomers into ordered multimers and amyloid fibrils. The present data suggest that the presence of glycans and GPI anchor do not cause a major restructuring of the underlying polypeptide backbone secondary structures within the 22L and ME7 PrP^{res} fibrils. However, the data do not negate the possibility that tertiary and quaternary structures might be affected significantly by glycans and anchors, or that the effects might be more significant with other prion strains.

Recent analyses of the rates of H/D exchange of the polypeptide backbone amide protons in infectious anchorless PrP^{res} fibrils has revealed extreme resistance to exchange throughout the entire proteinase K-resistant C-terminal portions of the PrP subunits (i.e., from residues ~80-90 to ~223) (42). These results strongly suggest that, contrary to previous IR-based reports (1;4;5;9), there is virtually no alpha helix in PrP^{res}. The previous reports employed different methods of estimating secondary structure compositions from IR spectra which were based on theoretical considerations and empirical calibrations using globular proteins of known structure. However, although such estimates are usually fairly accurate [e.g., (59)], they may at times be misleading due to ambiguities in band assignments or potential IR distortions due to poorly understood factors such as nonglobularity and/or oligomerization of particular protein samples (60). In any case, the fact that anchorless PrP^{res} appears to lack any of the alpha helices that are present in PrP^{C} raises the issue of whether wild type PrP^{res}, with its large hydrophilic glycans attached to Asn residues that are located on, or between, residues comprising helices 2 and 3 in PrP^{C}, also lacks those helices. Unfortunately, in the previous studies, the presence of the glycans prevented direct mass spectrometric analysis of H/D exchange in much of the proteinase K-resistant C-terminal region of wild type PrP^{res} (42). However, the close similarity of the IR spectra of anchorless and fully glycosylated wild type PrP^{res} that we have observed here strongly suggests that they have similar structures. Moreover, the spectra of the wild type PrP^{res} preparations gave no evidence for enhanced alpha helical content which, in PrP^{C} and many other proteins, absorb between 1650-1657 cm^{-1} (Figure 7). Indeed little, if any, banding in this latter spectral region was observed above the spectral noise for any of the PrP^{res} preparations. The adjacent band at 1659 cm^{-1} was prominent in both anchorless PrP^{res} preparations, which we have concluded has no alpha helices ; thus the 1659 cm^{-1} band is likely to be due to something other than alpha helix, such as turns. The prominence of the same band in wildtype PrP^{res}, and the relative lack of bands in the 1650-1657 cm^{-1} region lead us to surmise that, like their anchorless counterparts, wild type 22L and ME7 PrP^{res} fibrils have structures comprised predominantly of an extended solvent-inaccessible beta-sheeted core with occasional turns, but virtually no alpha helix.

Supplementary Material

Refer to Web version on PubMed Central for supplementary material.

Acknowledgments

Animal experiments were performed in accordance with animal welfare guidelines under an animal study protocol approved by the Animal Care and Use Committee of the Rocky Mountain Laboratories, National Institute of Allergy and Infectious Diseases, National Institutes of Health. The authors thank Mikael Klingeborn, Roger Moore, and Lara Taubner for critical reading of the manuscript.

REFERENCES

1. Pan K-M, Baldwin M, Nguyen J, Gasset M, Serban A, Groth D, Mehlhorn I, Huang Z, Fletterick RJ, Cohen FE, Prusiner SB. Conversion of alpha-helices into beta-sheets features in the formation of the scrapie prion protein. Proc. Natl. Acad. Sci. USA. 1993; 90:10962–10966. [PubMed: 7902575]
2. Riek R, Hornemann S, Wider G, Glockshuber R, Wuthrich K. NMR characterization of the full-length recombinant murine prion protein, mPrP(23-231). FEBS Lett. 1997; 413:282–288. [PubMed: 9280298]
3. Riek R, Hornemann S, Wider G, Billeter M, Glockshuber R, Wuthrich K. NMR structure of the mouse prion protein domain PrP(121-231). Nature. 1996; 382:180–182. [PubMed: 8700211]
4. Caughey BW, Dong A, Bhat KS, Ernst D, Hayes SF, Caughey WS. Secondary structure analysis of the scrapie-associated protein PrP 27-30 in water by infrared spectroscopy. Biochemistry. 1991; 30:7672–7680. [PubMed: 1678278]
5. Gasset M, Baldwin MA, Fletterick RJ, Prusiner SB. Perturbation of the secondary structure of the scrapie prion protein under conditions that alter infectivity. Proc. Natl. Acad. Sci. USA. 1993; 90:1–5. [PubMed: 8419912]
6. Safar J, Roller PP, Gajdusek DC, Gibbs CJ Jr. Conformational transitions, dissociation, and unfolding of scrapie amyloid (prion) protein. J. Biol. Chem. 1993; 268:20276–20284. [PubMed: 8104185]
7. Wuthrich K, Riek R. Three-dimensional structures of prion proteins. Adv. Prot. Chem. 2001; 57:55–82.
8. Lee S, Antony L, Hartmann R, Knaus KJ, Surewicz K, Surewicz WK, Yee VC. Conformational diversity in prion protein variants influences intermolecular beta-sheet formation. EMBO J. 2010; 29:251–262. [PubMed: 19927125]
9. Caughey B, Raymond GJ, Bessen RA. Strain-dependent differences in beta-sheet conformations of abnormal prion protein. J. Biol. Chem. 1998; 273:32230–32235. [PubMed: 9822701]
10. Thomzig A, Spassov S, Friedrich M, Naumann D, Beekes M. Discriminating scrapie and bovine spongiform encephalopathy isolates by infrared spectroscopy of pathological prion protein. J. Biol. Chem. 2004; 279:33847–33854. [PubMed: 15155741]
11. Spassov S, Beekes M, Naumann D. Structural differences between TSEs strains investigated by FT-IR spectroscopy. Biochim. Biophys. Acta. 2006; 1760:1138–1149. [PubMed: 16730908]
12. Kascsak RJ, Rubenstein R, Merz PA, Carp RI, Wisniewski HM, Diringer H. Biochemical differences among scrapie-associated fibrils support the biological diversity of scrapie agents. J. Gen. Virol. 1985; 66:1715–1722. [PubMed: 3926951]
13. Kascsak, RJ.; Rubenstein, R.; Carp, RI. Evidence for Biological and Structural Diversity Among Scrapie Strains. In: Chesebro, B., editor. Transmissible Spongiform Encephalopathies: Scrapie, BSE and Related Human Disorders. Springer-Verlag; Berlin-Heidelberg: 1991. p. 139-152.
14. Bessen RA, Marsh RF. Biochemical and physical properties of the prion protein from two strains of transmissible mink encephalopathy agent. J. Virol. 1992; 66:2096–2101. [PubMed: 1347795]
15. Bessen RA, Marsh RF. Distinct PrP properties suggest the molecular basis of strain variation in transmissible mink encephalopathy. J. Virol. 1994; 68:7859–7868. [PubMed: 7966576]
16. Bessen RA, Kocisko DA, Raymond GJ, Nandan S, Lansbury PT Jr. Caughey B. Nongenetic propagation of strain-specific phenotypes of scrapie prion protein. Nature. 1995; 375:698–700. [PubMed: 7791905]
17. Parchi P, Castellani R, Capellari S, Ghetti B, Young K, Chen SG, Farlow M, Dickson DW, Sima AAF, Trojanowski JQ, Petersen RB, Gambetti P. Molecular basis of phenotypic variability in sporadic Creutzfeldt-Jakob disease. Ann. Neurol. 1996; 39:767–778. [PubMed: 8651649]

18. Collinge J, Sidle KCL, Meads J, Ironside J, Hill AF. Molecular analysis of prion strain variation and the aetiology of “new variant” CJD. Nature. 1996; 383:685–690. [PubMed: 8878476]
19. Safar J, Wille H, Itri V, Groth D, Serban H, Torchia M, Cohen FE, Prusiner SB. Eight prion strains have PrP(Sc) molecules with different conformations. Nat. Med. 1998; 4:1157–1165. [see comments]. [PubMed: 9771749]
20. Fernie K, Steele PJ, Taylor DM, Somerville RA. Comparative studies on the thermostability of five strains of transmissible-spongiform-encephalopathy agent. Biotechnol. Appl. Biochem. 2007; 47:175–183. [PubMed: 17331068]
21. Wille H, Michelitsch MD, Guenebaut V, Supattapone S, Serban A, Cohen FE, Agard DA, Prusiner SB. Structural studies of the scrapie prion protein by electron crystallography. Proc. Natl. Acad. Sci. U. S. A. 2002; 99:3563–3568. [PubMed: 11891310]
22. Wille H, Govaerts C, Borovinskiy A, Latawiec D, Downing KH, Cohen FE, Prusiner SB. Electron crystallography of the scrapie prion protein complexed with heavy metals. Arch. Biochem. Biophys. 2007; 467:239–248. [PubMed: 17935686]
23. Sim VL, Caughey B. Ultrastructures and strain comparison of under-glycosylated scrapie prion fibrils. Neurobiol. Aging. 2009; 30:2031–2042. [PubMed: 18394757]
24. Caughey B, Race RE, Ernst D, Buchmeier MJ, Chesebro B. Prion protein (PrP) biosynthesis in scrapie-infected and uninfected neuroblastoma cells. J. Virol. 1989; 63:175–181. [PubMed: 2562814]
25. Hay B, Barry RA, Lieberburg I, Prusiner SB, Lingappa VR. Biogenesis and transmembrane orientation of the cellular isoform of the scrapie prion protein. Mol. Cell. Biol. 1987; 7:914–920. [PubMed: 3547085]
26. Stahl N, Borchelt DR, Hsiao K, Prusiner SB. Scrapie prion protein contains a phosphatidylinositol glycolipid. Cell. 1987; 51:229–240. [PubMed: 2444340]
27. Vorberg I, Priola SA. Molecular basis of scrapie strain glycoform variation. J. Biol. Chem. 2002; 277:36775–36781. [PubMed: 12138171]
28. Neuendorf E, Weber A, Saalmueller A, Schatzl H, Reifenberg K, Pfaff E, Groschup MH. Glycosylation deficiency at either one of the two glycan attachment sites of cellular prion protein preserves susceptibility to bovine spongiform encephalopathy and scrapie infections. J. Biol. Chem. 2004; 279:53306–53316. [PubMed: 15448157]
29. Tuzi NL, Cancellotti E, Baybutt H, Blackford L, Bradford B, Plinston C, Coghill A, Hart P, Piccardo P, Barron RM, Manson JC. Host PrP glycosylation: a major factor determining the outcome of prion infection. PLoS. Biol. 2008; 6:e100. [PubMed: 18416605]
30. Cancellotti E, Bradford BM, Tuzi NL, Hickey RD, Brown D, Brown KL, Barron RM, Kisielewski D, Piccardo P, Manson JC. Glycosylation of PrPC determines timing of neuroinvasion and targeting in the brain following transmissible spongiform encephalopathy infection by a peripheral route. J. Virol. 2010; 84:3464–3475. [PubMed: 20106922]
31. Lawson VA, Priola SA, Wehrly K, Chesebro B. N-terminal truncation of prion protein affects both formation and conformation of abnormal protease-resistant prion protein generated in vitro. J. Biol. Chem. 2001; 276:35265–35271. [PubMed: 11466311]
32. Winklhofer KF, Heller U, Reintjes A, Tatzelt J. Inhibition of complex glycosylation increases the formation of PrPsc. Traffic. 2003; 4:313–322. [PubMed: 12713659]
33. Piro JR, Harris BT, Nishina K, Soto C, Morales R, Rees JR, Supattapone S. Prion protein glycosylation is not required for strain-specific neurotropism. J. Virol. 2009; 83:5321–5328. [PubMed: 19297485]
34. Chesebro B, Trifilo M, Race R, Meade-White K, Teng C, LaCasse R, Raymond L, Favara C, Baron G, Priola S, Caughey B, Masliah E, Oldstone M. Anchorless prion protein results in infectious amyloid disease without clinical scrapie. Science. 2005; 308:1435–1439. [PubMed: 15933194]
35. Chesebro B, Race B, Meade-White K, LaCasse R, Race R, Klingeborn M, Striebel J, Dorward D, McGovern G, Jeffrey M. Fatal transmissible amyloid encephalopathy: a new type of prion disease associated with lack of prion protein membrane anchoring. PLoS. Pathog. 2010; 6:e1000800. [PubMed: 20221436]

36. Klingeborn M, Race B, Meade-White KD, Rosenke R, Striebel JF, Chesebro B. Crucial Role for Prion Protein Membrane Anchoring in the Neuroinvasion and Neural Spread of Prion Infection. J. Virol. 2011; 85:1484–1494. [PubMed: 21123371]
37. Kocisko DA, Come JH, Priola SA, Chesebro B, Raymond GJ, Lansbury PT, Caughey B. Cell-free formation of protease-resistant prion protein. Nature. 1994; 370:471–474. [PubMed: 7913989]
38. Walmsley AR, Zeng F, Hooper NM. Membrane topology influences N-glycosylation of the prion protein. EMBO J. 2001; 20:703–712. [PubMed: 11179215]
39. Beekes M, Lasch P, Naumann D. Analytical applications of Fourier transform-infrared (FT-IR) spectroscopy in microbiology and prion research. Vet. Microbiol. 2007; 123:305–319. [PubMed: 17540519]
40. Mishra RS, Basu S, Gu Y, Luo X, Zou WQ, Mishra R, Li R, Chen SG, Gambetti P, Fujioka H, Singh N. Protease-resistant human prion protein and ferritin are cotransported across Caco-2 epithelial cells: implications for species barrier in prion uptake from the intestine. J. Neurosci. 2004; 24:11280–11290. [PubMed: 15601934]
41. Raymond, GJ.; Chabry, J. Purification of the pathological isoform of prion protein (PrPSc or PrPres) from transmissible spongiform encephalopathy-affected brain tissue. In: Lehmann, S.; Grassi, J., editors. Techniques in Prion Research. Birkhauser Verlag; Basel: 2004. p. 16-26.
42. Smirnovas V, Baron GS, Offerdahl DK, Raymond GJ, Caughey B, Surewicz WK. Structural organization of brain-derived mammalian prions examined by hydrogen-deuterium exchange. Nat. Struct. Mol. Biol. 2011; 18:504–506. [PubMed: 21441913]
43. Blum H, Beier H, Gross HJ. Improved silver staining of plant proteins, RNA and DNA in polyacrylamide gels. Electrophoresis. 1987; 8:93–99.
44. Atarashi R, Wilham JM, Christensen L, Hughson AG, Moore RA, Johnson LM, Onwubiko HA, Priola SA, Caughey B. Simplified ultrasensitive prion detection by recombinant PrP conversion with shaking. Nat. Methods. 2008; 5:211–212. [PubMed: 18309304]
45. Race B, Meade-White K, Oldstone MB, Race R, Chesebro B. Detection of prion infectivity in fat tissues of scrapie-infected mice. PLoS. Pathog. 2008; 4:e1000232. [PubMed: 19057664]
46. Moore RA, Timmes A, Wilmarth PA, Priola SA. Comparative profiling of highly enriched 22L and Chandler mouse scrapie prion protein preparations. Proteomics. 2010; 10:2858–2869. [PubMed: 20518029]
47. Russelakis-Carneiro M, Hetz C, Maundrell K, Soto C. Prion replication alters the distribution of synaptophysin and caveolin 1 in neuronal lipid rafts. Am. J. Pathol. 2004; 165:1839–1848. [PubMed: 15509552]
48. Naslavsky N, Stein R, Yanai A, Friedlander G, Taraboulos A. Characterization of detergent-insoluble complexes containing the cellular prion protein and its scrapie isoform. J. Biol. Chem. 1997; 272:6324–6331. [PubMed: 9045652]
49. Meier P, Genoud N, Prinz M, Maissen M, Rulicke T, Zurbriggen A, Raeber AJ, Aguzzi A. Soluble dimeric prion protein binds PrP(Sc) in vivo and antagonizes prion disease. Cell. 2003; 113:49–60. [PubMed: 12679034]
50. Hnasko R, Serban AV, Carlson G, Prusiner SB, Stanker LH. Generation of antisera to purified prions in lipid rafts. Prion. 2010; 4:94–104. [PubMed: 20647769]
51. Madore N, Smith KL, Graham CH, Jen A, Brady K, Hall S, Morris R. Functionally different GPI proteins are organized in different domains on the neuronal surface. EMBO J. 1999; 18:6917–6926. [PubMed: 10601014]
52. Chen X, Jen A, Warley A, Lawrence MJ, Quinn PJ, Morris RJ. Isolation at physiological temperature of detergent-resistant membranes with properties expected of lipid rafts: the influence of buffer composition. Biochem. J. 2009; 417:525–533. [PubMed: 18831713]
53. Taylor CM, Coetzee T, Pfeiffer SE. Detergent-insoluble glycosphingolipid/cholesterol microdomains of the myelin membrane. J. Neurochem. 2002; 81:993–1004. [PubMed: 12065611]
54. Atarashi R, Sim VL, Nishida N, Caughey B, Katamine S. Prion strain-dependent differences in conversion of mutant prion proteins in cell culture. J. Virol. 2006; 80:7854–7862. [PubMed: 16873242]
55. Callahan MA, Xiong L, Caughey B. Reversibility of scrapie-associated prion protein aggregation. J. Biol. Chem. 2001; 276:28022–28028. [PubMed: 11375994]

56. Rauber NR, Jany KD, Pfleiderer G. Ribonuclease A digestion by proteinase K. Z. Naturforsch. C. 1978; 33:660–663. [PubMed: 153663]

57. Townsend MW, DeLuca PP. Stability of ribonuclease A in solution and the freeze-dried state. J. Pharm. Sci. 1990; 79:1083–1086. [PubMed: 2079655]

58. Libonati M, Gotte G. Oligomerization of bovine ribonuclease A: structural and functional features of its multimers. Biochem. J. 2004; 380:311–327. [PubMed: 15104538]

59. Dong A, Huang P, Caughey WS. Protein secondary structures in water from second-derivative amide I infrared spectra. Biochemistry. 1990; 29:3303–3308. [PubMed: 2159334]

60. Surewicz WK, Mantsch HH, Chapman D. Determination of protein secondary structure by Fourier transform infrared spectroscopy: a critical assessment. Biochemistry. 1993; 32:389–394. [PubMed: 8422346]

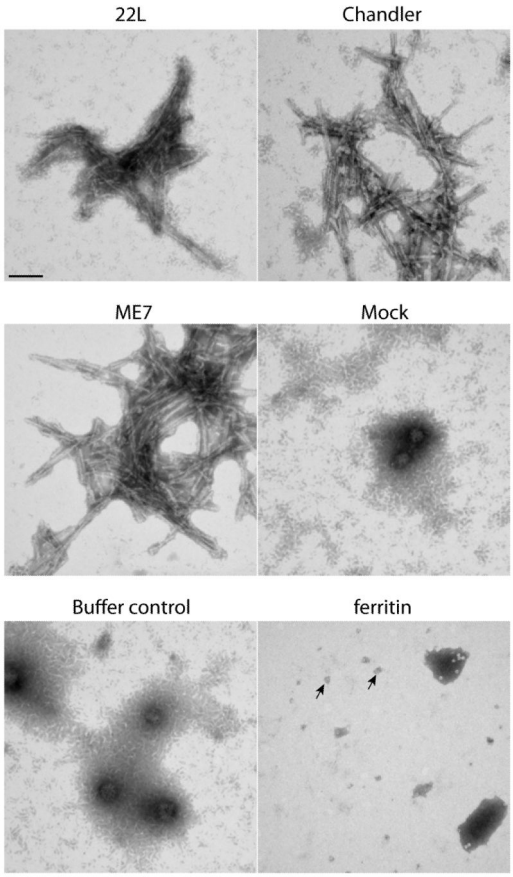

Figure 1.
Ultrastructure of anchorless PrP^{res} fibrils. Samples were stained with methylamine tungstate and examined by TEM. Images of mock anchorless PrP^{res}, buffer, and purified mouse ferritin are shown as controls. Arrows, ferritin particles. Bar, 100 nm.

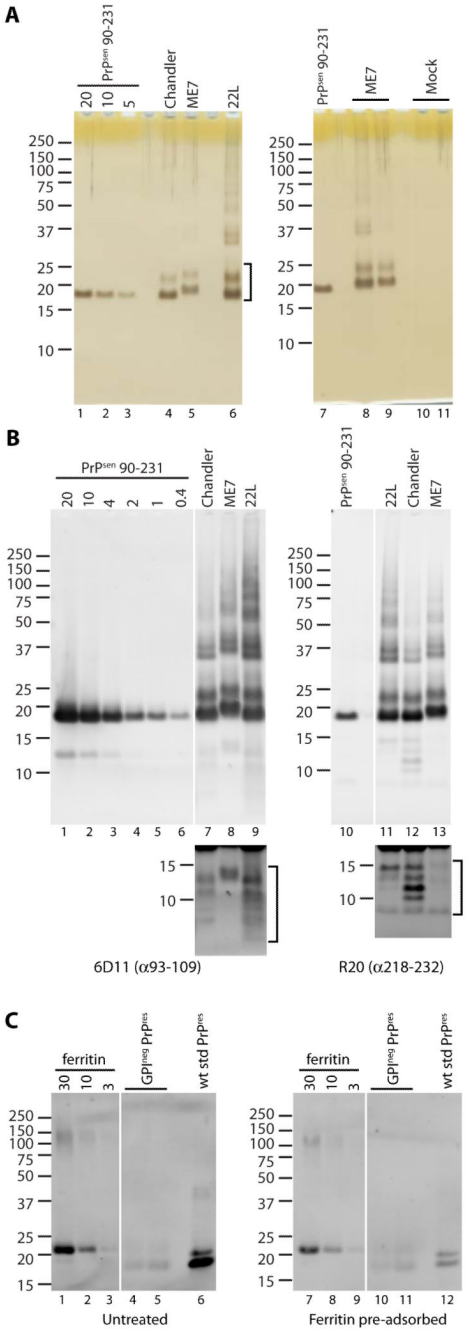

Figure 2.

Biochemical characterization of anchorless PrP^{res} preparations. (A) Silver-stained SDS-PAGE gels. Varying amounts of hamster $rPrP^{sen}$ 90-231 (ng) were loaded as indicated (lanes 1-3). Lanes 8-9 and 10-11 each represent samples from independent preparations. Bracket indicates bands corresponding to anchorless PrP^{res} monomers. (B) Immunoblot analysis with 6D11 or R20 anti-PrP antibodies. Varying amounts of hamster $rPrP^{sen}$ 90-231 (ng) were loaded as indicated (lanes 1-6). Brackets (lower panels) indicate strain-specific low molecular mass species. (C) Immunoblot with anti-heavy chain ferritin antibody. Blots were performed using antibody without (Untreated) or with (Ferritin pre-adsorbed) pre-adsorption with purified mouse ferritin to determine ferritin-specific antibody binding.

Varying amounts of purified mouse liver ferritin (ng) were loaded as indicated (lanes 1-3 and 7-9). GPI^{neg} PrP^{res}, two independent preparations of anchorless 22L PrP^{res} containing either 1.2 (lanes 4 and 10) or 2 μg (lanes 5 and 11) of PrP^{res}. wt std PrP^{res}, 300 ng of wt 22L PrP^{res} prepared by a standard method (41). For (A)-(C), molecular mass standards are indicated on the left (kDa) and white lines indicate removal of irrelevant lanes.

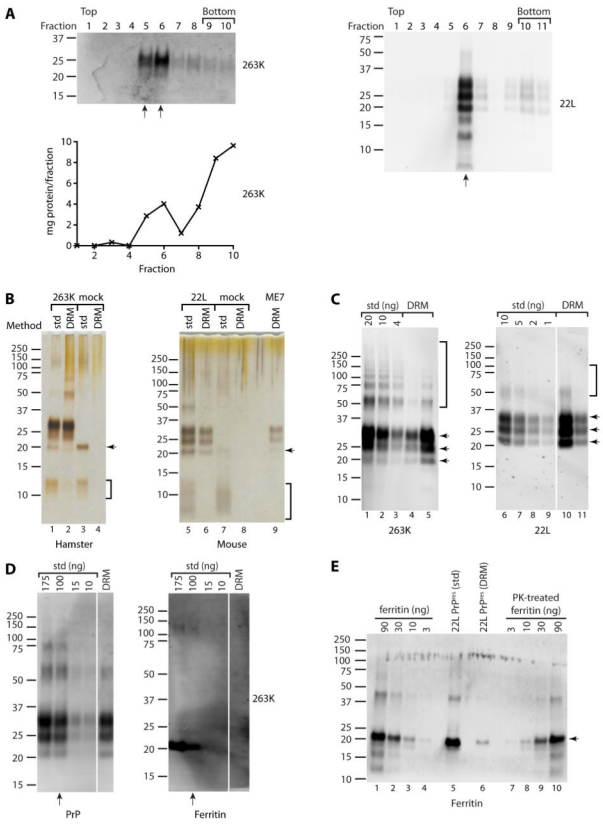

Figure 3.

Biochemical characterization of wt PrP^{res} preparations. (A) PrP^{res} enriched in brain DRM fractions. Immunoblot analysis (with 6D11 antibody) of PK-treated fractions from brain DRM preparations from hamsters (263K) or mice (22L) infected with rodent scrapie. Arrows indicate DRM band fractions (fractions 5-6). Fractions 2-3 correspond to a second major lipid band of lower buoyant density observed in the gradient. Graph shows distribution of total protein across fractions from 263K brain DRM gradient. (B) Silver-stain SDS-PAGE gel analysis of PrP^{res} preparations from hamsters and mice using the standard method (std) versus the DRM method (DRM). Similar amounts of std and DRM PrP^{res} were loaded based on PrP content. Control mock preparations from hamsters or mice are shown for comparison. Std and DRM mock PrP^{res} samples (lanes 3-4 and 7-8) were normalized to each other based on brain equivalents. Arrow, ferritin band present in mock and scrapie PrP^{res} preparations using the standard method. Brackets, low molecular mass species that are significantly reduced in DRM PrP^{res} preparations. (C) Immunoblot analysis (6D11 antibody) of PrP^{res} preparations. Varying amounts of std PrP^{res} (ng) were loaded as indicated (lanes 1-3 and 6-9). Arrows indicate the three major glycoforms of PrP. Brackets, SDS-resistant PrP^{res} oligomers. (D) Immunoblots of 263K PrP^{res} with anti-PrP (R20) and anti-heavy chain ferritin antibodies. Varying amounts of std 263K PrP^{res} (ng) were loaded as indicated. Ferritin was not detected in the DRM PrP^{res} prep (DRM) but readily detected in a std PrP^{res} prep with comparable loading for PrP (arrows). (E) Immunoblot of 22L PrP^{res} with anti-heavy chain ferritin antibody. Dilution series of purified mouse ferritin without (lanes 1-4) or with PK treatment (7-10) were loaded as indicated. Lanes 5 and 6 contain 150 ng of either std or DRM 22L PrP^{res}, respectively. Arrow, ferritin monomer. SDS-resistant ferritin oligomers are also visible. For (A)-(E), molecular mass standards are indicated on the left (kDa) and white lines indicate removal of irrelevant lanes.

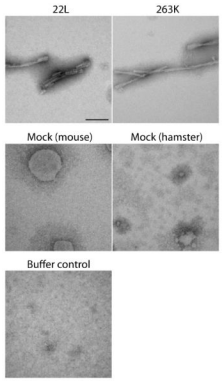

Figure 4.

Ultrastructure of wt DRM PrP^{res} fibrils. Samples were stained with ammonium molybdate and examined by TEM. Grids of mock DRM PrP^{res} from mice or hamsters were exposed to 10-fold more brain equivalents than 263K or 22L PrP^{res} grids to compensate for the extremely low levels of material in mock PrP^{res} samples. Bar, 100 nm.

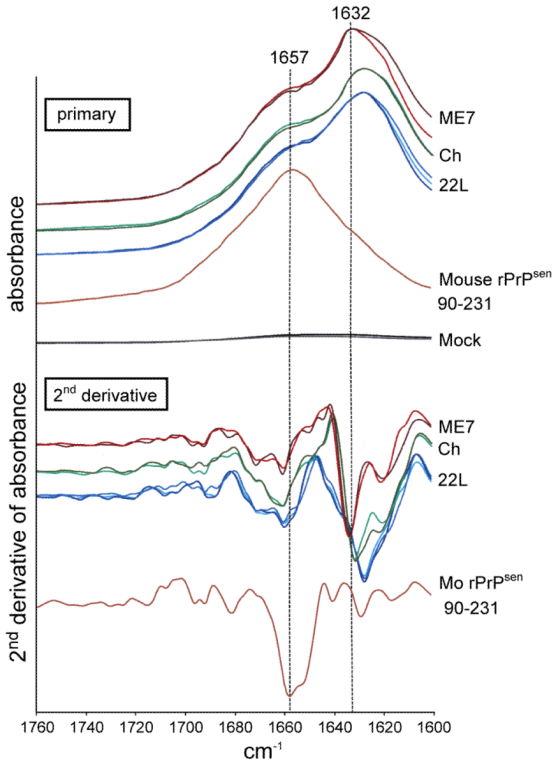

Figure 5.

IR spectra of anchorless PrP^{res} (murine ME7, Chandler, and 22L strains) and recombinant PrP^{sen} 90-231. Individual primary (top) and second derivative (bottom) IR spectra represent independent preparations. For comparison, a spectrum of comparable brain equivalents of a mock anchorless PrP^{res} preparation from normal brain tissue is shown. The spectra of the PrP^{res} preparations have been normalized to one another so that the absorbance terms are arbitrary. The Chandler spectra are the same as those presented elsewhere in a different context as Supplemental Data (42).

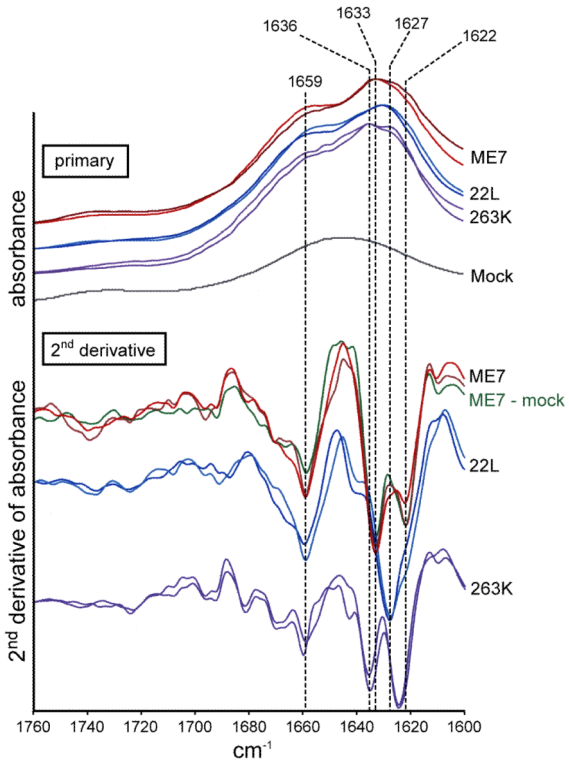

Figure 6.

IR spectra of wild type PrP^{res} (mouse ME7 and 22L, hamster 263K strains). Individual primary (top) and second derivative (bottom) spectra represent independent preparations. Comparable brain equivalent of a mock wild type PrP^{res} preparation from normal brain tissue is shown as well as a second derivative spectrum calculated from an ME7-mock difference spectrum (green). Compared to the PrP^{res} spectra, the mock spectrum also displayed a much reduced relative absorbance in the protein amide II region (~1545 cm^{-1}, not shown) suggesting that the absorbance at ~1650 cm^{-1} is due predominantly to something other than protein. The spectra of the PrP^{res} preparations have been normalized to one another so that the absorbance terms are arbitrary.

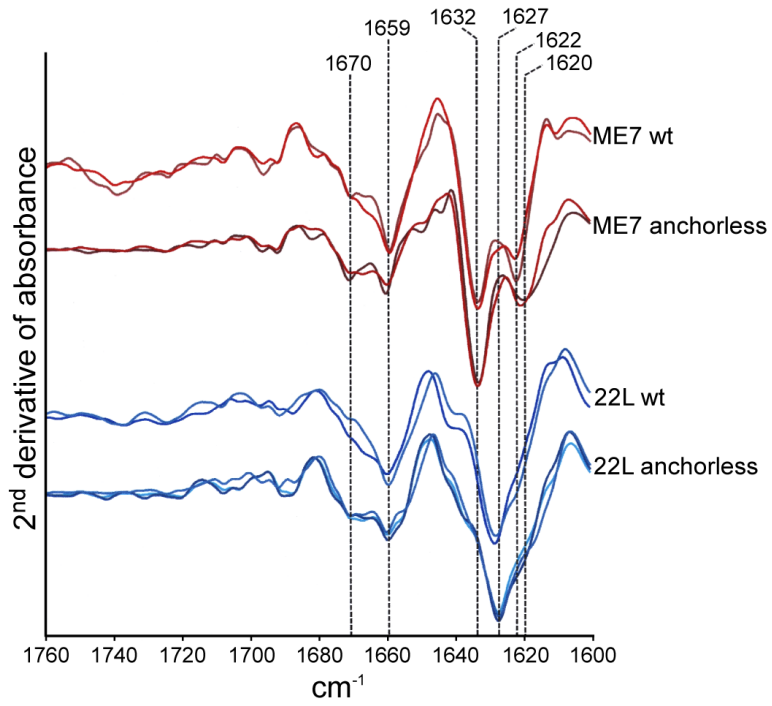

Figure 7.
Comparisons of anchorless and wild type PrP^{res} second derivative IR spectra.